# A Modified Semivectorial BPM Retaining the Effects of the Longitudinal Field Component and Its Application to the Design of a Spot-Size Converter

NAKANO, Hisamatsu / YAMAUCHI, Junji / NITO, Yuta

(出版者 / Publisher)
Institute of Electrical and Electronics Engineers
(雑誌名 / Journal or Publication Title)
Journal of lightwave technology / Journal of lightwave technology
(号 / Number)
13
(開始ページ / Start Page)
2470
(終了ページ / End Page)
2476
(発行年 / Year)
2009-07-01

# A Modified Semivectorial BPM Retaining the Effects of the Longitudinal Field Component and Its Application to the Design of a Spot-Size Converter

Junji Yamauchi, *Senior Member, IEEE, Member, OSA*, Yuta Nito, and Hisamatsu Nakano, *Fellow, IEEE*

***Abstract*—For the analysis of a $z$-variant optical waveguide with high-index contrast by the beam-propagation method (BPM), the error often grows up during the propagation process. In this paper, the formulation of the BPM is revisited, taking into account the effects of the longitudinal field component. The improvement in accuracy is demonstrated through the analysis of a vertically tapered rib waveguide. The power expression based on the Poynting vector is also employed to improve the power conservation property. As an application, the present technique is applied to the design of a spot-size converter composed of a multicore structure. It is numerically demonstrated that the use of a curvilinearly tapered core leads to a conversion length of 570 $\mu$m, which is 42% less than the length of a linearly tapered core, with a coupling efficiency of 97% being maintained at a wavelength of 1.55 $\mu$m.**

***Index Terms*—Beam-propagation method (BPM), power conservation, spot-size converter (SSC).**

## I. Introduction

THE analysis of an optical waveguide with high-index contrast by the beam-propagation method (BPM) is a challenging task in terms of accuracy and power conservation [1]. The difficulty becomes significant particularly when a waveguide with an asymmetrical index profile is treated. To resolve this problem, some attempts were made, but most of the previous works neglected the existence of the longitudinal field components [2]–[4], except for the full vectorial treatment done by Montanari *et al.* [5]. In this paper, we newly formulate a semivectorial BPM partially retaining the effects of the longitudinal field component [6]. The power is evaluated on the basis of the Poynting vector. The improvement in terms of accuracy and power conservation is demonstrated through the analysis of a vertically tapered rib waveguide. Some numerical results obtained with the finite-difference time-domain (FDTD) method are also presented to clarify the motivation of revisiting the BPM formulation.

As an application of the present BPM, we analyze a spot-size converter (SSC). Many types of SSCs were designed using a tapered waveguide [7]–[12]. Watanabe *et al.* [10] have developed the SSC composed of a multicore structure, in which a strongly guiding core with a linear taper is loaded on a weakly guiding core. In this paper, we investigate the SSC using the present BPM to design an optimum taper configuration. It is numerically demonstrated that the use of a curvilinearly tapered core leads to a conversion length of 570 $\mu$m, which is 42% less than the length of a linearly tapered core, with a coupling efficiency of 97% being maintained at a wavelength of 1.55 $\mu$m.

Manuscript received October 22, 2008; revised December 11, 2008. First published April 17, 2009; current version published July 01, 2009. This work was supported by MEXT Grant-in-Aid for Scientific Research (C) (19560355).

The authors are with the Faculty of Engineering, Hosei University, Koganei, Tokyo 184-8584, Japan (e-mail: j.yma@k.hosei.ac.jp; yuta.nito.lt@gs-eng.hosei.ac.jp; hymat@hosei.ac.jp).

Color versions of one or more of the figures in this paper are available online at http://ieeexplore.ieee.org.

Digital Object Identifier 10.1109/JLT.2008.2011496

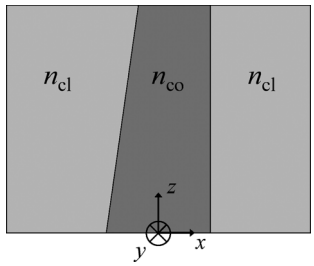


Fig. 1. Configuration of a 2-D tapered slab waveguide.

## II. Inference From a Planar Structure

In this section, we infer appropriate field components to be used in the 3-D BPM analysis from the field components used in the analysis of a 2-D planar structure.

We consider a 2-D slab waveguide whose refractive index varies slowly towards the $z$-direction, as shown in Fig. 1. For the transverse-magnetic (TM) mode, the magnetic field component does not exist in the longitudinal direction $(H_z = 0)$. Furthermore, $H_x = E_y = 0$, so that we can only treat the $E_x$, $E_z$, and $H_y$ components. This means that the TM wave can be analyzed correctly by using only the magnetic field $(H_y)$ component. Similarly, for the transverse-electric (TE) mode, there exists the $E_y$, $H_x$, and $H_z$ components. Therefore, the TE wave can be analyzed by using only the electric field $(E_y)$ component. In other words, the propagating field can be analyzed by using the components tangential to the core-cladding interface whose refractive index varies along the $z$-direction. From this fact, we can expect the situation in a 3-D structure whose refractive index varies only in the horizontal or vertical plane. Since the longitudinal field components are neglected in the conventional semivectorial BPM, we have to select the $E$ or $H$ field whose longitudinal component is sufficiently small. As a result, it is expected that the BPM gives fairly good results, provided the field component tangential to the core-cladding interface whose refractive index varies along the $z$-direction is chosen.

To clarify the aforementioned inference, we perform the FDTD analysis of the vertically tapered rib waveguide shown in Fig. 2, since the FDTD method provides the variation of all

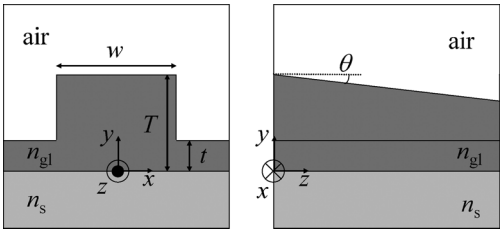


Fig. 2. Configuration of a tapered rib waveguide.

the field components. The rib waveguide is the same as that used in a benchmark test [13], and its configuration parameters are $n_{\rm gl} = 3.44$, $n_{\rm s} = 3.40$, rib width $w = 3.0\ \mu$m, central rib height $T = 1.0\ \mu$m, and lateral height $t = 0.2\ \mu$m. The taper angle is taken to be $\theta = 1.0°$ and the wavelength is chosen to be $\lambda = 1.15\ \mu$m. Spatial sampling widths are $\Delta x = 0.05\ \mu$m and $\Delta y = \Delta z = 0.025\ \mu$m. The boundary between the guiding layer and the air region is expressed by the staircase approximation. Higdon's absorbing boundary condition [14] is employed for the FDTD analysis throughout this paper.

Fig. 3 shows the squared norms of the minor components as a function of propagation distance for the $H^x$ (quasi-TM) and the $H^y$ (quasi-TE) modes, respectively. The electric and magnetic fields are normalized in such a way that their magnitudes are of the same order [15]. It is seen that the norm of the $E_z$ component increases during the propagation process for the $H^x$ mode [Fig. 3(a)]. This means that the analysis of the quasi-TM mode using only the $E_y$ component is not suitable, since the $E_z$ component is neglected in the conventional BPM. Fig. 3(a) also shows that neglecting the minor transverse components is reasonable. Consequently, we should use the $H_x$ component for analyzing the quasi-TM mode in this configuration. On the other hand, the norm of the $H_z$ component increases during the propagation process for the $H^y$ mode [Fig. 3(b)], so that we should use the $E_x$ component in the analysis of the quasi-TE mode.

Preliminary BPM analysis confirms that the results obtained with the components normal to a variant core-cladding interface induce larger errors than those with the components tangential to the interface. This fact is noticeable in the analysis using the $E$ field components. We, therefore, extend our discussion on the basis of the $H$ field in the following sections.

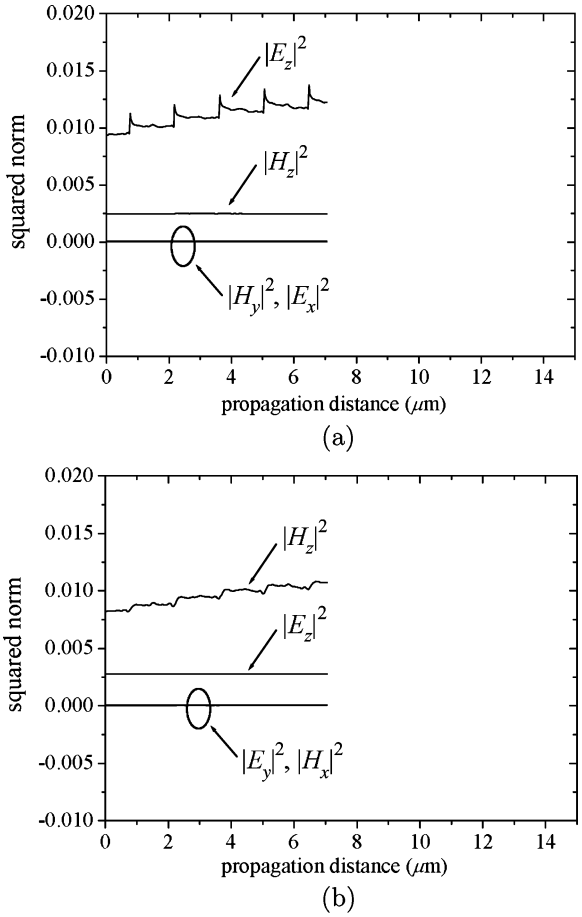


Fig. 3. Squared norms of minor components versus propagation distance. (a) $H^x$ mode. (b) $H^y$ mode. The calculation is done until 7 $\mu$m due to the limited computer memory.

## III. Formulation

### A. Modified Semivectorial BPM

From the discussion in Section II, it can be said that the use of the field components tangential to a variant core-cladding interface is reasonable for the semivectorial BPM analysis. It should be noted, however, that the refractive index of some optical waveguides varies both horizontally and vertically. This fact motivates us to develop a BPM that takes into account the effects of the longitudinal field component, since it is expected to allow the use of the field component normal to the variant core-cladding interface. In this section, we will develop a modified semivectorial BPM that partially takes into account the effects of the $H_z$ component.

We start from Maxwell's equations

$$\nabla \times \mathbf{E} = -j\omega\mu_0\mathbf{H} \tag{1}$$

$$\nabla \times \mathbf{H} = j\omega\varepsilon_0 n^2\mathbf{E} \tag{2}$$

where $\varepsilon_0$ and $\mu_0$ are the free-space permittivity and permeability, respectively. $\omega$ is the angular frequency and $n = n(x, y, z)$ is the refractive index profile of a waveguide. By eliminating $\mathbf{E}$ from Maxwell's equations, we obtain the vector wave equation

$$\nabla^2\mathbf{H} + \frac{\nabla n^2}{n^2} \times (\nabla \times \mathbf{H}) + k_0^2 n^2 \mathbf{H} = 0 \tag{3}$$

where $k_0$ is the free-space wavenumber. Most of the previous works have neglected the term $\partial_z n^2$ in (3), since $z$-invariant waveguides or slowly $z$-variant waveguides are assumed. This approximation, which implies the negligence of the longitudinal field components, often induces numerical errors.

We now treat the $H^y$ mode. Since the negligence of the minor transverse components is reasonable in the tapered structure, we formulate propagation equations with retaining $\partial_z n^2$. Expressing the field $\mathbf{H}$ as $\mathbf{H} = \boldsymbol{H}\exp(-jk_0 n_0 z)$ with $n_0$ being the reference refractive index, we obtain a set of coupled equations in terms of the $H_y$ and $H_z$ components

$$\begin{aligned} &2jk_0 n_0 \frac{\partial H_y}{\partial z} - \frac{\partial^2 H_y}{\partial z^2} \\ &\quad = n^2 \frac{\partial}{\partial x}\left(\frac{1}{n^2}\frac{\partial H_y}{\partial x}\right) + \frac{\partial^2 H_y}{\partial y^2} \\ &\qquad + \left\{k_0^2\left(n^2 - n_0^2\right) + jk_0 n_0 \frac{1}{n^2}\frac{\partial n^2}{\partial z}\right\} H_y \end{aligned}$$

$$+\frac{1}{n^2}\frac{\partial n^2}{\partial z}\frac{\partial H_z}{\partial y} \tag{4}$$

$$2jk_0n_0\frac{\partial H_z}{\partial z}-\frac{\partial^2 H_z}{\partial z^2} = n^2\frac{\partial}{\partial x}\left(\frac{1}{n^2}\frac{\partial H_z}{\partial x}\right)+\frac{\partial^2 H_z}{\partial y^2} +\left\{k_0^2\left(n^2-n_0^2\right)-\frac{1}{n^2}\frac{\partial n^2}{\partial y}\frac{\partial}{\partial y}\right\}H_z -jk_0n_0\frac{1}{n^2}\frac{\partial n^2}{\partial y}H_y. \tag{5}$$

Note that the necessity of the term $(jk_0n_0/n^2\partial n^2/\partial z)H_y$ in (4) (corresponding to the term #A in (7)) has already been pointed out in [1] and [2]. To evaluate the $H_z$ component of the last term in (4), we employ the relation $\nabla\cdot\mathbf{H}=0$. After expressing the field $\mathbf{H}=\boldsymbol{H}\exp(-jk_0n_0z)$ and substituting this equation into the divergence equation, we have

$$H_z=\frac{1}{jk_0n_0}\left(\frac{\partial H_x}{\partial x}+\frac{\partial H_y}{\partial y}+\frac{\partial H_z}{\partial z}\right). \tag{6}$$

It should be noted that within the framework of the slowly varying envelope approximation (SVEA), the $H$ field satisfies the relation $|k_0n_0H|\gg|\partial H/\partial z|$. Also recall that $H_x\simeq 0$ for the $H^y$ mode. This means that the first and third terms in (6) can be omitted. The resultant equation can be substituted into (4). Interestingly enough, the introduction of the SVEA into the $H_z$ component leads to decoupling of the $H_y$ and $H_z$ components, so that the following modified propagation equation consisting only of the $H_y$ component is derived

$$2jk_0n_0\frac{\partial H_y}{\partial z}-\frac{\partial^2 H_y}{\partial z^2} = n^2\frac{\partial}{\partial x}\left(\frac{1}{n^2}\frac{\partial H_y}{\partial x}\right)+\left(1+\underbrace{\frac{1}{jk_0n_0}\frac{1}{n^2}\frac{\partial n^2}{\partial z}}_{\#\mathrm{B}}\right)\frac{\partial^2 H_y}{\partial y^2} +\left\{k_0^2\left(n^2-n_0^2\right)+\underbrace{jk_0n_0\frac{1}{n^2}\frac{\partial n^2}{\partial z}}_{\#\mathrm{A}}\right\}H_y. \tag{7}$$

Note that the term #B appears by the effect of the $H_z$ component.

To evaluate the second derivative with respect to the transverse direction, we employ the second-order finite-difference scheme [2], which takes into account the boundary condition at the dielectric interface. The terms #A and #B in (7) are evaluated using the following formula [16]:

$$\frac{1}{n_l^2}\frac{\partial n_l^2}{\partial z}=-n_l^{-2}\frac{\partial n_l}{\partial z} \simeq -2n_l^2\frac{1/\left(n_{l+1}^2+n_l^2\right)-1/\left(n_l^2+n_{l-1}^2\right)}{\Delta z} \tag{8}$$

where $l$ indicates the position along the $z$-direction. Another scheme, such as the use of a natural logarithm, may also be used instead of (8), and almost the same results are obtained in the present tapered rib waveguide. Our previous study showed that (8) may yield better results, depending on the problem [2].

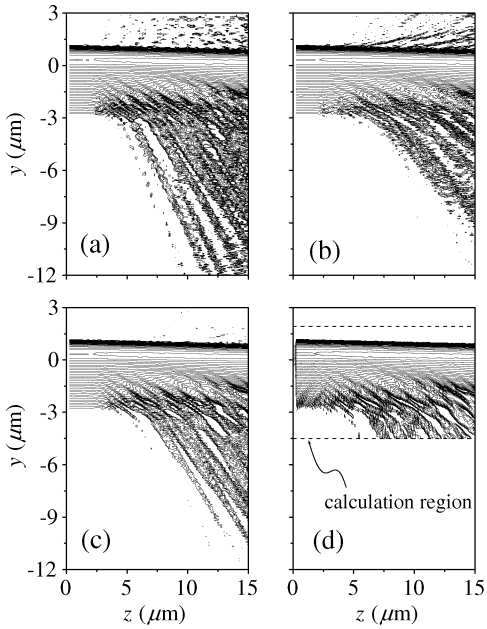


Fig. 4. Field distributions for $H^y$ mode. (a) Without #A and #B. (b) With #A. (c) With #A and #B. (d) FDTD analysis.

We carry out the propagating beam analysis to verify the accuracy of the derived propagation equation. Here, we apply the Padé approximant only to the vertical direction using the paraxial approximation to the horizontal direction and employ the alternating-direction implicit method [17], so that

First step

$$\left[1+\frac{j\Delta z}{4k_0n_0}D_{xx}\right]H_y^{l+1/2}=\left[1+\left(\frac{1}{4k_0^2n_0^2}-\frac{j\Delta z}{4k_0n_0}\right)\times\left(D_{yy}+\nu+jk_0n_0\partial_z n^2\right)\right]H_y^l. \tag{9}$$

Second step

$$\left[1+\left(\frac{1}{4k_0^2n_0^2}+\frac{j\Delta z}{4k_0n_0}\right)\left(D_{yy}+\nu+jk_0n_0\partial_z n^2\right)\right]H_y^{l+1}=\left[1-\frac{j\Delta z}{4k_0n_0}D_{xx}\right]H_y^{l+1/2} \tag{10}$$

where

$$\nu=k_0^2\left(n^2-n_0^2\right)$$

$$D_{xx}=n^2\frac{\partial}{\partial x}\left(\frac{1}{n^2}\frac{\partial}{\partial x}\right)$$

$$D_{yy}=\left(1+\frac{1}{jk_0n_0}\frac{1}{n^2}\frac{\partial n^2}{\partial z}\right)\frac{\partial^2}{\partial y^2}$$

$$\partial_z n^2=\frac{1}{n^2}\frac{\partial n^2}{\partial z}.$$

We analyze the vertically tapered rib waveguide under the condition of the same sampling widths as those in the FDTD analysis. The reference refractive index is chosen to be $n_0=\beta/k_0$, where $\beta$ is the propagation constant of the waveguide at $z=0$ $\mu$m.

The calculated field distributions are shown in Fig. 4. The field is expressed by a logarithmic scale, in which the data up to $-45$ dB are presented. Appreciable numerical noise is found for the conventional formulation without the terms #A and #B

[Fig. 4(a)]. The inclusion of the term #A reduces error, but the numerical noise remains in the air region [Fig. 4(b)]. Introduction of both terms #A and #B greatly contributes to a reduction in the numerical noise [Fig. 4(c)]. For further comparison, we show the field distribution obtained from the FDTD method [Fig. 4(d)], in which the calculation is done only within the region shown by the broken line due to the limited computer memory [$\Delta z = 0.05\ \mu$m is used only for Fig. 4(d)]. From these figures, good agreement is found to exist between the results obtained from the modified BPM and FDTD method.

### *B. Power Evaluation Based on the Poynting Vector*

Next, we investigate the power evaluation based on the Poynting vector [6]. The Poynting vector is defined as

$$P = \frac{1}{2}\int\int \mathrm{Re}(\mathbf{E}\times\mathbf{H}^*)\cdot\mathbf{n}_z dxdy = \frac{1}{2}\int\int \mathrm{Re}\left(\mathrm{E}_x\mathrm{H}_y^* - \mathrm{E}_y\mathrm{H}_x^*\right) ds \tag{11}$$

where the superscript * denotes the complex conjugate. From (2), the $E_x$ and $E_y$ components are expressed as

$$\mathrm{E}_x = \frac{1}{j\omega\varepsilon_0 n^2}\left(\frac{\partial \mathrm{H}_z}{\partial y} - \frac{\partial \mathrm{H}_y}{\partial z}\right) \tag{12}$$

$$\mathrm{E}_y = \frac{1}{j\omega\varepsilon_0 n^2}\left(\frac{\partial \mathrm{H}_x}{\partial z} - \frac{\partial \mathrm{H}_z}{\partial x}\right). \tag{13}$$

Substituting (12) and (13) into (11), we obtain

$$P_H = \frac{1}{2j\omega\varepsilon_0}\int\int \frac{1}{n^2}\mathrm{Re}\left[\left(\frac{\partial \mathrm{H}_z}{\partial y} - \frac{\partial \mathrm{H}_y}{\partial z}\right)\mathrm{H}_y^* - \left(\frac{\partial \mathrm{H}_x}{\partial z} - \frac{\partial \mathrm{H}_z}{\partial x}\right)\mathrm{H}_x^*\right] dxdy. \tag{14}$$

Again expressing the field as $\mathbf{H} = \boldsymbol{H}\exp(-jk_0n_0z)$, the power is given by

$$P_H = \frac{1}{2\omega\varepsilon_0}\int\int \frac{1}{n^2}\mathrm{Re}\left[\underbrace{-jH_y^*\frac{\partial H_z}{\partial y}}_{\#1} \underbrace{+jH_y^*\frac{\partial H_y}{\partial z}}_{\#2} \underbrace{+jH_x^*\frac{\partial H_x}{\partial z}}_{\#3} \underbrace{-jH_x^*\frac{\partial H_z}{\partial x}}_{\#4} + k_0n_0\left(\underbrace{H_yH_y^*}_{\#5} + \underbrace{H_xH_x^*}_{\#6}\right)\right] dxdy. \tag{15}$$

In the conventional scheme, only the term #5 or #6 in (15) is evaluated, often resulting in nonconservation of power.

We again deal with the vertically tapered rib waveguide discussed so far. Fig. 5 shows the contribution of each term in (15) obtained with the FDTD method. Since the term #3 retains the appreciable magnitude for the $H^x$ mode, the evaluation of the term #3 as well as the major term #6 is expected to contribute to improving the power conservation property. It is found in Fig. 5(b) that the major term #5 exhibits some humps for the $H^y$ mode. The locations of the humps correspond to the index change caused by the staircase approximation. It should be noted that the term #1 generated by the longitudinal field component varies so as to compensate the variation of the major term #5. Therefore, the term #1 must also be evaluated in addition to the terms #2 and #5.

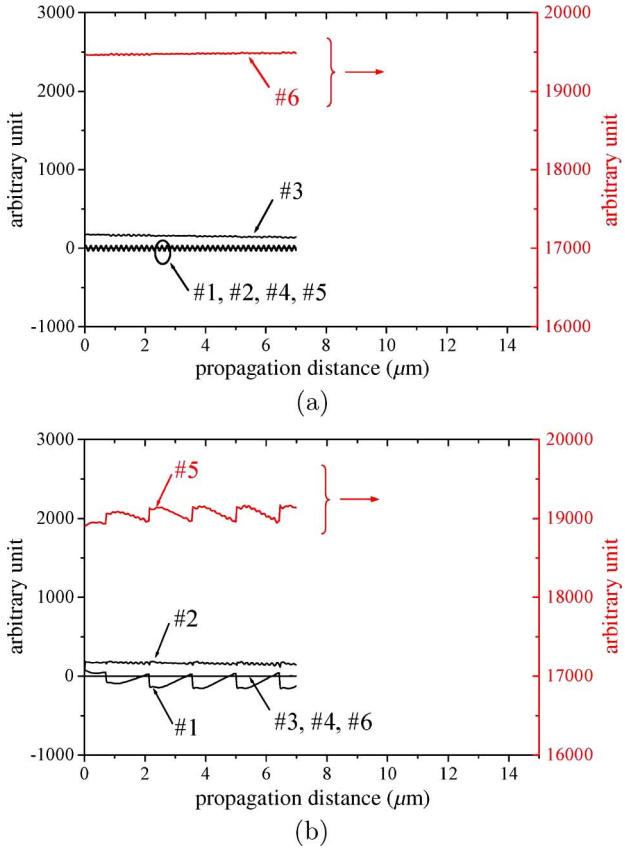


Fig. 5. Decomposition of power obtained by Poynting vector. (a) $H^x$ mode. (b) $H^y$ mode.

Fig. 6 shows the normalized power obtained with the BPM analysis. The notations in the brackets mean the terms in (15) used in the power evaluation. To check the power conservation property, we intentionally eliminate the absorbing boundary condition. Since the power is normalized to the input power, the power should retain unity provided the power conservation property is maintained.

It is found from Fig. 6(a) that the use of the $H_x$ component, which is tangential to the variant core-cladding interface, together with the evaluation of the terms #3 and #4, contributes to improving the power conservation property. We should recall that the contribution of the term #4 is negligible for the $H^x$ mode, so that the evaluation of the term #4 is not necessarily required.

In contrast to Fig. 6(a), Fig. 6(b) indicates that the use of the $H_y$ component, which is normal to the variant core-cladding interface, results in the appreciable humps in the normalized power evaluated by the major term #5, corresponding to those observed in Fig. 5(b). However, the evaluation of the terms #A and #B, together with the terms #1, and #2 and #5, considerably serves to keep the normalized power constant.

## IV. Design of a SSC

We apply the present BPM to designing the SSC shown in Fig. 7(a), which was developed in [10]. The SSC is composed of a multicore structure, in which a strongly guiding core with

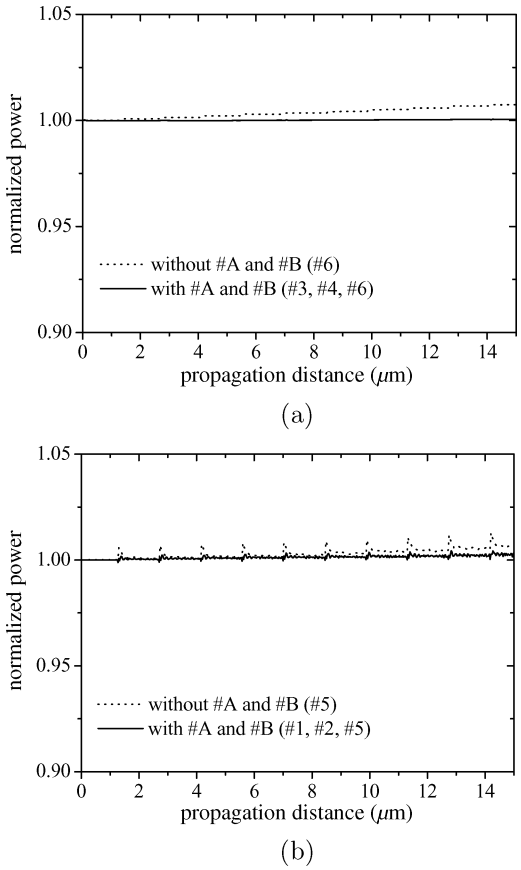


Fig. 6. Normalized power versus propagation distance. (a) $H^x$ mode. (b) $H^y$ mode.

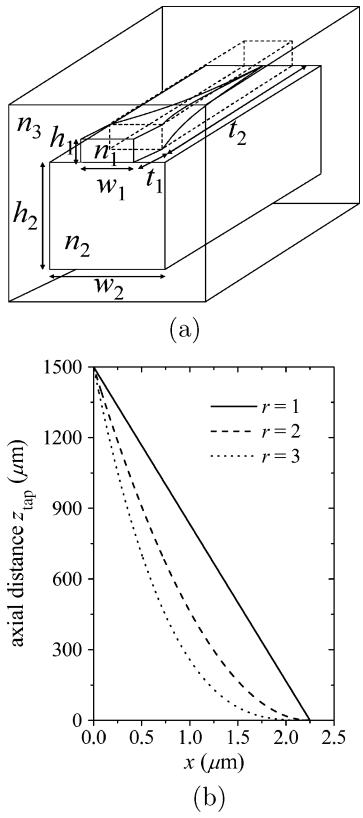


Fig. 7. SSC. (a) Perspective view. (b) Taper profiles.

a taper profile is loaded on a weakly guiding core. The configuration parameters of the upper core are taken as follows: the refractive index $n_1 = 1.4824$, width $w_1 = 4.5\ \mu$m, and height $h_1 = 2.0\ \mu$m, while those in the lower core are $n_2 = 1.4644$, $w_2 = 8.0\ \mu$m, and $h_2 = 8.0\ \mu$m. The refractive index of the cladding is chosen to be $n_3 = 1.46$. The wavelength is chosen to be $\lambda = 1.55\ \mu$m and consideration is given to the $H^y$ mode. The sampling widths are taken to be $\Delta x = \Delta y = 0.05\ \mu$m, and $\Delta z = 0.5\ \mu$m. The eigenmode analysis shows that the present SSC is intended to convert the $1/e^2$ spot-size from 16.8 $\mu$m$^2$ to 85.2 $\mu$m$^2$.

In [10], only a linearly tapered core was studied. In this paper, we consider the taper structure in more detail. The tapered profile of the upper core width, $w(z_{\rm tap})$, is expressed as [18]

$$w(z_{\rm tap}) = \frac{w_1}{2} - \left(\frac{w_1}{2}\right)\left(\frac{z_{\rm tap}}{t_2}\right)^{1/r} \tag{16}$$

where $z_{\rm tap}$ is the axial distance of the tapered section. The overall length of the tapered section is fixed to be $t_2 = 1500\ \mu$m and the length of the straight section $t_1$ is varied. The upper core is also tapered vertically in the same manner as the horizontal direction. Changing the parameter $r$ in (16) allows us to control a taper shape, as shown in Fig. 7(b). The waveguide with $r = 1$ is linearly tapered, which corresponds to the configuration proposed in [10], and that with $r > 1$ is curvilinearly tapered.

To confirm the power conservation property, we first analyze the linearly tapered SSC using the technique in Section III (the Padé approximant is applied only to the vertical direction since larger field variation is observed in the vertical plane). Fig. 8 shows the normalized power as a function of propagation distance. From the figure, it is found that the evaluation of neglected terms (#A, #B, #1, and #2) serves to conserve the power, although not completely. Fig. 8 demonstrates that the present technique can be used for a structure tapered both vertically and horizontally.

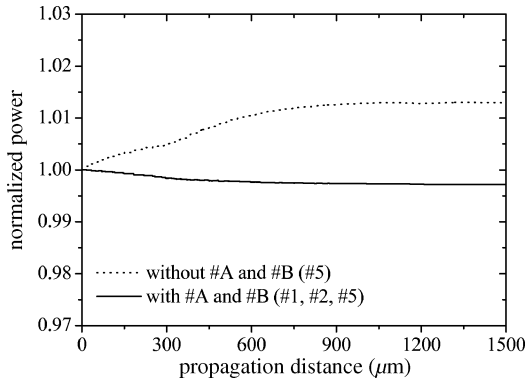


Fig. 8. Normalized power ($r = 1$ and $t_1 = 0\ \mu$m).

We now consider the coupling characteristics between the upper and lower cores of the SSC. To obtain smooth power transfer from the upper core to the lower core, we have to consider two factors: one is the suppression of generating the radiation modes along the tapered core and the other is the adjustment of the coupling length between the two cores.

Note that Ladouceur and Love [19] intuitively described a low-loss criterion for a taper profile of a dielectric-waveguide: Radiation loss will be small if the taper length is large compared with the coupling length between the fundamental guided-mode and the radiation field. The limit of the local taper angle $(\Omega(z_{\rm tap}))$ between the $z$-axis and the tangent to the dielectric interface was expressed as

$$\Omega(z_{\rm tap}) = \tan^{-1}\frac{w(z_{\rm tap})\,[k_z(z_{\rm tap}) - k_{\rm cl}]}{2\pi} \simeq \frac{w(z_{\rm tap})\,[k_z(z_{\rm tap}) - k_{\rm cl}]}{2\pi} \tag{17}$$

where $k_z(z_{\rm tap})$ is the propagation constant of the upper core at $z_{\rm tap}$, and $k_{\rm cl}$ is that in the cladding. This equation implies that the change in $w(z_{\rm tap})$ should become less for larger $z_{\rm tap}$. Therefore, the guided-mode power is expected to be maintained in a curvilinear taper compared with a linear taper.

We also note that the coupling between the upper and lower cores is determined by the even and odd supermodes, since the SSC can be regarded as a composite waveguide. If the phase matching between the two cores is satisfied, the power in the upper core is completely converted into the lower core, although a long distance is required. On the other hand, if the phase matching is not fully satisfied, only part of the power is transferred to the lower core, with the coupling length being relatively short. We should recall that the propagation constant of the upper core is varied depending on its cross section. Since the propagation constant of the upper core at the input is larger than that of the lower core, the coupling length around the input is relatively short with an insufficient power transfer to the lower core. As the cross section of the upper core is decreased, the coupling length becomes long and the coupling efficiency increases because the propagation constant of the upper core approaches that of the lower core.

Keeping the aforementioned discussion in mind, we turn to the propagating beam analysis. Fig. 9 shows the coupling efficiency as a function of propagation distance when the SSC is excited with the fundamental mode of the upper core. The coupling efficiency is calculated by the guided-mode power of the lower core. The length of the straight section of the upper core is fixed to be $t_1 = 0\ \mu$m. For $r = 1$ the oscillatory behavior at short propagation distances is observed as the field propagates, since the coupling length between the upper and lower cores is too short near the input region. The coupling efficiency is calculated to be 97% at a propagation distance of $z = 980\ \mu$m. On the other hand, the comparable efficiency can be obtained at a shorter length of $z = 890\ \mu$m for $r = 2$, since the curvilinear taper makes the coupling length longer with subsequent suppression of the oscillatory behavior near the input region. In the case of $r = 3$, the radiation loss increases due to the excessive taper of the upper core, resulting a low coupling efficiency.

To further facilitate the smooth transfer of the power from the upper core into the lower core, the straight waveguide, whose length is designated as $t_1$, may be employed at the input region. Fig. 10 shows the coupling efficiency as a function of propagation distance, in which $t_1$ is varied (the taper shape parameter is fixed to be $r = 2$). A coupling efficiency of 97% can be obtained at a propagation distance of $z = 570\ \mu$m when we choose

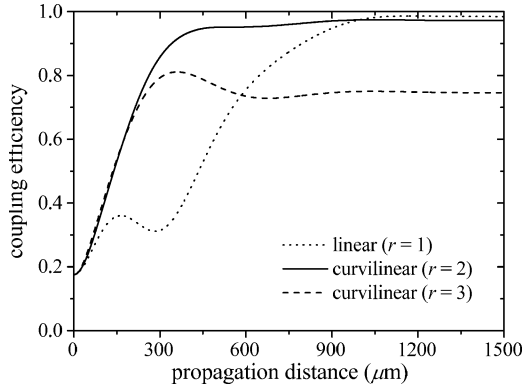


Fig. 9. Coupling efficiency $(t_1 = 0\ \mu$m$)$.

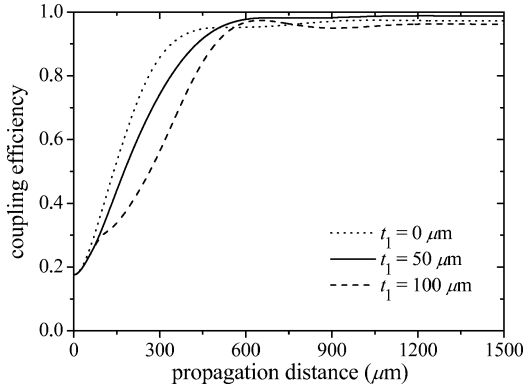


Fig. 10. Coupling efficiency $(r = 2)$.

$t_1 = 50\ \mu$m. Although not shown, the characteristics of the $H^x$ mode are similar to those of the $H^y$ mode.

## V. Conclusion

We have developed a modified semivectorial BPM, which partially takes into account the effects of the longitudinal field component. The motivation of revisiting the formulation of the BPM is described on the basis of the results obtained with the FDTD method. After indicating the effectiveness of the use of the field components tangential to a variant core-cladding interface, we show that the inclusion of the longitudinal field component leads to improvement in accuracy for the analysis of a step-index waveguide by the field component normal to the variant core-cladding interface.

The power evaluation based on the Poynting vector is also carried out to show the contribution of all the field components to the total power. The results obtained with the FDTD method clearly indicates the necessity of the inclusion of some terms neglected in conventional schemes.

As an application, a SSC composed of a multicore structure, in which the upper core is tapered both horizontally and vertically, is analyzed to design an optimum taper configuration. It is numerically demonstrated that the use of a curvilinearly tapered core leads to a conversion length of 570 $\mu$m, which is 42% less than the length of a linearly tapered core, with a coupling efficiency of 97% being maintained at a wavelength of 1.55 $\mu$m.

Finally, we add a brief comment on the treatment where the transverse minor component cannot be negligible. In this case,

the equation corresponding to (7) becomes coupled ones, including the $H_x$ and $H_y$ components. Furthermore, we have to evaluate all the terms appeared in the power evaluation of (15). Although we have already implemented this kind of full-vectorial scheme and confirmed its effectiveness in the analysis of a polarization rotator [20], the detailed discussion will be presented in a separate paper.

## REFERENCES


[1] C. Vassallo, "Difficulty with vectorial BPM," *Electron. Lett.*, vol. 33, no. 1, pp. 61–62, Jan. 1997.

[2] J. Yamauchi, K. Matsubara, T. Tsuda, and H. Nakano, "Norm-conserving finite-difference beam propagation method for TM wave analysis in step-index waveguides," *J. Lightw. Technol.*, vol. 18, no. 5, pp. 721–728, 2000.

[3] P. L. Ho and Y. Y. Lu, "Improving the beam propagation method for TM polarization," *Opt. Quantum Electron.*, vol. 35, no. 4, pp. 507–519, 2003.

[4] J. Yamauchi, K. Sumida, and H. Nakano, "Analysis of a polarization splitter with a multilayer filter using a Padé-operator-based power-conserving fourth-order accurate beam-propagation method," *IEEE Photon. Technol. Lett.*, vol. 18, no. 17, pp. 1858–1860, Sep. 2006.

[5] E. Montanari, S. Selleri, L. Vincetti, and M. Zoboli, "Finite-element full-vectorial propagation analysis for three-dimensional $z$-varying optical waveguides," *J. Lightw. Technol.*, vol. 16, no. 4, pp. 703–714, 1998.

[6] J. Yamauchi, Y. Nito, and H. Nakano, "A modified semivectorial beam-propagation method retaining the longitudinal field component," in *Proc. Integ. Photon. Nanophoton. Res. Appl.*, Boston, MA, Jul. 2008, paper IWB5.

[7] P. Sewell, T. M. Benson, and P. C. Kendall, "Rib waveguide spot-size transformers: Modal properties," *J. Lightw. Technol.*, vol. 17, no. 5, pp. 848–856, 1999.

[8] T. Bakke, C. T. Sullivan, and S. D. Mukherjee, "Polymeric optical spot-size transformer with vertical and lateral tapers," *J. Lightw. Technol.*, vol. 20, no. 7, pp. 1188–1197, 2002.

[9] T. Kitoh, M. Ishii, Y. Inoue, T. Saida, M. Itoh, T. Shibata, and Y. Hibino, "Compact and low-loss arrayed waveguide grating module with tolerance-relaxed spot-size converter," *IEEE Photon. Technol. Lett.*, vol. 15, no. 2, pp. 239–241, Feb. 2003.

[10] K. Watanabe, Y. Nakanishi, I. Ogawa, M. Kohtoku, and Y. Inoue, "Multi-core spot size converter integrated silica based waveguide for laser diode coupling," in *Proc. Commun. Gen. Conf. IEICE*, Suita, Japan, Mar. 2005, C-3-81.

[11] S. Haxha, E. O. Ladely, M. Mjeku, F. AbdelMalek, and B. M. A. Rahman, "Optimization of compact lateral, vertical, and combined tapered spot-size converters by use of the beam-propagation method," *Appl. Opt.*, vol. 45, no. 2, pp. 288–296, Jan. 2006.

[12] D. Dai, S. He, and H. Tsang, "Bilevel mode converter between a silicon nanowire waveguide and a larger waveguide," *J. Lightw. Technol.*, vol. 24, no. 6, pp. 2428–2433, 2006.

[13] C. Vassallo, "1993–1995 optical mode solvers," *Opt. Quantum Electron.*, vol. 29, no. 2, pp. 95–114, 1997.

[14] R. L. Higdon, "Absorbing boundary conditions for difference approximations to the multidimensional wave equation," *Math. Comput.*, vol. 47, no. 176, pp. 437–459, 1986.

[15] S. T. Chu, W. P. Huang, and S. K. Chaudhuri, "Simulation and analysis of waveguide based optical integrated circuits," *Comput. Phys. Commun.*, vol. 68, no. 1–3, pp. 451–484, 1991.

[16] C. Vassallo, "Finite difference analysis of vectorial transversal fields in optical waveguides," in *Proc. 3rd Int. Conf. Math. Numerical Aspects Wave Propag. (SIAM-INRIA)*, Mandelieu, Apr. 1995, pp. 594–603.

[17] J. Shibayama, T. Takahashi, J. Yamauchi, and H. Nakano, "A three-dimensional horizontally wide-angle noniterative beam-propagation method based on the alternating-direction implicit scheme," *IEEE Photon. Technol. Lett.*, vol. 18, no. 5, pp. 661–663, Mar. 2006.

[18] T. Ando, I. Ohba, S. Numata, J. Yamauchi, and H. Nakano, "Linearly and curvilinearly tapered cylindrical dielectric-rod antennas," *IEEE Trans. Antennas Propag.*, vol. 53, no. 9, pp. 2827–2832, Sep. 2005.

[19] F. Ladouceur and J. D. Love, *Silica-Based Buried Channel Waveguides and Devices*. London, U.K.: Chapman & Hall, 1996.

[20] Y. Nito, J. Yamauchi, and H. Nakano, "Power-conserving full-vectorial FD-BPM including the $z$-derivative of refractive index," in *Proc. Commun. Gen. Conf. IEICE*, Ehime, Japan, Mar. 2009, C-3-74.


**Junji Yamauchi** (M'84–SM'08) was born in Nagoya, Japan, on August 23, 1953. He received the B.E., M.E., and Dr.Eng. degrees from Hosei University, Tokyo, Japan, in 1976, 1978, and 1982, respectively.

From 1984 to 1988, he served as a Lecturer in the Electrical Engineering Department of Tokyo Metropolitan Technical College. Since 1988, he has been a member of the faculty of Hosei University, where he is now a Professor. His research interests include optical waveguides and circularly polarized antennas. He is the author of *Propagating Beam Analysis of Optical Waveguides* (Research Studies Press, 2003).

Dr. Yamauchi is a member of the Optical Society of America and the Institute of Electronics, Information and Communication Engineers of Japan.

**Yuta Nito** was born in Kanagawa, Japan, on November 13, 1984. He received the B.E. degree from Hosei University, Tokyo, Japan, in 2007, where he is currently working toward the M.E. degree.

Mr. Nito is a Student Member of the Institute of Electronics, Information and Communication Engineers (IEICE) of Japan.

**Hisamatsu Nakano** (M'75–SM'87–F'92) was born in Ibaraki, Japan, on April 13, 1945. He received his B.E., M.E., and Dr.Eng. degrees in electrical engineering from Hosei University, Tokyo, Japan, in 1968, 1970, and 1974, respectively.

Since 1973, he has been a member of the faculty of Hosei University, where he is now a Professor of electronic informatics. His research topics include numerical methods for low- and high-frequency antennas and optical waveguides. He has published more than 200 refereed journal papers, more than 200 international symposium papers, and more than 750 national symposium papers. He is the author of a book entitled *Helical and Spiral Antennas* (Wiley, 1987) and the coauthor of *Analysis Methods of Electromagnetic Wave Problems*, Volume Two (Artech House, 1986). In addition, he is the author of *Helical and Spiral Antennas, Encyclopedia of Communications* (Wiley, 2002). He is an Associate Editor of several journals and magazines, such as *Electromagnetics*, IEEE ANTENNAS AND PROPAGATION MAGAZINE, IEEE ANTENNAS AND WIRELESS PROPAGATION LETTERS, and *Asian Information-Science-Life*.

Dr. Nakano received the IEE International Conference on Antennas and Propagation Best Paper Award and the IEEE TRANSACTIONS ON ANTENNAS AND PROPAGATION Best Application Paper Award (H. A. Wheeler Award) in 1989 and 1994, respectively. In 1992, he was elected as an IEEE Fellow for contributions to the design of spiral and helical antennas. In 2001, he received the Award of Distinguished Technical Communication (from the Society for Technical Communication, USA) and the Science and Technology Progress Award (from Hangzhou, China). He was also the recipient of the Chen-To Tai Distinguished Educator Award (from the IEEE Antennas and Propagation Society) in 2006.